A General Method for the Synthesis of Nanostructured Large-Surface-Area Materials through the Self-Assembly of Functionalized Nanoparticles

Jean-Yves Chane-Ching,*[a] Frederic Cobo,[a] Daniel Aubert,[a] Howard G. Harvey,[a] Marc Airiau,[a] and Avelino Corma[b]

Abstract: A general synthetic method for the preparation of nanostructured materials with large surface area was developed by using nanoparticle building blocks. The preparation route involves the self-assembly of functionalized nanoparticles in a liquid-crystal phase. These nanoparticles are functionalized by using difunctional amino acid species to provide suitable interactions with the template. Optimum interactions for self-assembly of the nanoparticles in the liquid-crystal phase were achieved with one -NH_2 group anchored to the nanoparticle surface per 25 Å^2. To maximize the surface area of these materials, the wall thicknesses are adjusted so that they are composed of a monolayer of nanoparticles. To form such materials, numerous parameters have to be controlled such as the relative volume fraction of the nanoparticles and the template and size matching between the hydrophilic component of the copolymer and nanoparticles. The surface functionalization renders our synthetic route independent of the nanoparticles and allows us to prepare a variety of nanostructured composite materials that consist of a juxtaposition of different discrete oxide nanoparticles. Examples of such materials include CeO_2, ZrO_2, and CeO_2–$Al(OH)_3$ composites.

Keywords: composites · nanoparticles · nanostructures · self-assembly

Introduction

Thermally stable, ordered, crystalline inorganic nanostructured and mesoporous materials of large surface area are of importance in the fields of, catalysis,[1] separation,[2] sorption,[3] sensing,[4] and fuel cells.[5] A large range of silica-based[6] and non-siliceous[7–9] mesoporous materials, such as alumina, titania, niobia, tantala, and other mixed oxides, are generally synthesized by precipitation from supersaturated solutions, by using ordered arrays of surfactants as templates. Precipitation routes are best suited to siliceous materials, which are thermally stable up to 800 °C.[10] Non-siliceous mesoporous materials are often more difficult to synthesize by precipitation routes and often exhibit poor crystallinity and low thermal stability. Methods of strengthening the mesostructured walls include increasing their thicknesses,[7] exchanging surface sulfate groups for other species such as phosphate in the case of mesostructured ZrO_2,[11] and using $[Al_{13}O_4(OH)_{24}(OH_2)_{12}]^{7+}$ polycationic species as structural building blocks to form rigid Al_2O_3 frameworks.[12] Crystalline non-siliceous mesoporous frameworks, such as CeO_2,[13] yttria–zirconia or ceria–zirconia[14] have recently been prepared by a judicious choice of surfactants, inorganic salts, or the presence of large inorganic walls. However, the preparation of non-siliceous mesostructured composites containing two different materials have not been achieved by precipitation routes. Success has been obtained by performing post-synthetic doping; however, this results in a disordered distribution of the dopant.

Alternative pathways to the formation of nanostructured materials involve the spatial patterning of inorganic nanoparticles using template-directed construction.[15–16] Templates such as bacterial threads[17] and polymer gels[18] have been used with the goal of constructing materials with long-range organization. However, the resultant products have been found to retain the characteristic shape and length of the organic templates and do not generally display large surface areas and pore volumes. Large-surface-area crystalline oxides, with wormlike morphologies, have previously been synthesized by using ultra-fine colloidal nanoparticles as

[a] Dr. J.-Y. Chane-Ching, F. Cobo, D. Aubert, Dr. H. G. Harvey, M. Airiau
Rhodia Recherches, 52 Rue de la Haie Coq
93308- Aubervilliers (France)
Fax: (+33) 149-376-489
E-mail: jean-yves.chane-ching@eu.rhodia.com

[b] Prof. Dr. A. Corma
Instituto de Tecnologia Quimica, UPV-CSIC, Avd de los Naranjos
46022, Valencia (Spain)

building blocks and a block copolymer as a template. However, the preparation route uses meta-tungstate anions as an interaction-promoting additive and all the resultant materials were found to irreversibly incorporate large amounts of WO_3.[19]

There is a need for a versatile route to manufacture nanostructured materials with large surface areas, particularly one that yields ordered nanostructured composite materials consisting of a juxtaposition of nanodomains of different compositions.

Here we report on a general and versatile synthetic route for the synthesis of ordered crystalline nanostructured oxides using ultrafine colloidal nanoparticles as building blocks and liquid-crystal templates. Our method is based upon the cooperative self-assembly of colloidal nanoparticles and a copolymer surfactant, and is driven by weakly attractive interactions. These weak interactions between the surfaces of the nanoparticles and the template were adjusted by post modification of the nanoparticle surfaces. Our synthetic method involves the functionalization of the nanoparticle surfaces, and, because of the interactions between tailored chemical moieties anchored to the nanoparticle surfaces and an organic template, our self-assembly process is independent of the nature of the nanoparticle building block. Thus, it is possible to say the functionalization of the nanoparticle surfaces renders them suitable for interaction with organic surfactants so that they self-assemble upon solvent evaporation (a concentration process) to form open nanostructured materials with large surface areas. The organic moieties were selected such that they possess one terminal group that interacts specifically with the nanoparticle surfaces. An amino group was selected for the other terminal group, which interacts with the (CH_2CH_2O) groups of the surfactant. By virtue of this functionalization of the nanoparticle surfaces we can fabricate not only nanostructured materials, but also composite nanostructures formed from various combinations of functionalized nanoparticles.

Results and Discussion

The desired properties of the synthesized solids include large surface areas and high thermal stability. These properties can be achieved for a nanostructured material by controlling the wall thicknesses. This can be adjusted by synthesizing such materials with walls consisting of a monolayer of nanoparticles. The optimum wall thickness is in the range of 3–5 nm, since it provides a compromise in terms of both high thermal stabilities and large surface areas. Nanoparticles of these diameters were therefore selected.

Our synthetic method involves a self-assembly process with the slow evaporation of water from a homogeneous dispersion of colloidal nanoparticles and copolymer surfactant (Figure 1). The copolymer surfactants used were poly(alkylene oxide) block copolymers possessing CH_2CH_2O groups.

Several factors must be considered when forming nanostructured materials from nanoparticle building blocks.

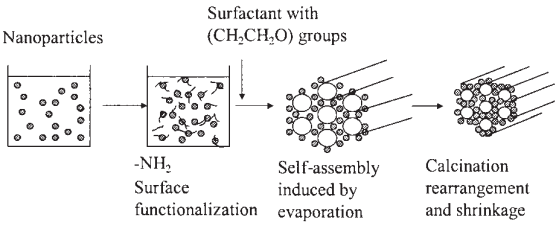

Figure 1. Synthetic route for the self-assembly of surface-modified nanoparticles

1) The self-assembly process, from which the nanostructured materials are formed, requires a colloidal dispersion of individualized nanoparticles. Colloidal dispersions of perfectly individualized CeO_2, ZrO_2, and $Al(OH)_3$ nanoparticles, possessing positively charged surfaces and diameters in the range of 3–5 nm, were used.
2) The organic moieties to be anchored on the nanoparticle surfaces must be selected for the specific nanoparticle materials, for example, carboxylic groups were chosen to bind to the surfaces of CeO_2, and sulfonate groups were chosen to bind to the surfaces of $Al(OH)_3$ and ZrO_2. We therefore selected aminocaproic acid and taurine as complexing agents. The organic anchors are terminated with amino groups in each case due to a favorable interaction between the amine groups and the copolymer across a wide range of pH values. The nanoparticle surface coverage was then optimized by adjusting the molar ratio [amine]/[M_xO_y].
3) The inter-nanoparticle interactions have to be adjusted to avoid uncontrolled nanoparticle flocculation. This was achieved by increasing the magnitude of the repulsive inter-nanoparticle interactions by lowering the ionic strength of the colloidal dispersion. Purification of the colloidal dispersions was performed by using an ultra-filtration step after the surface modification step.
4) The respective volumes of the nanoparticle and copolymer template must be carefully manipulated to form a monolayer nanostructure.

The original symmetry is preserved in all cases upon calcination of the materials and, in most examples, hexagonal symmetry is observed by transmission electron microscopy (TEM) in the uncalcined and calcined materials. The small-angle X-ray scattering (SAXS) peaks with a d_{SAXS} value can then be correlated to a lattice parameter a, assuming hexagonal symmetry, by the equation $a = 2d_{SAXS}/\sqrt{3}$. A value for the pore diameter of the material, determined from BET analysis, can then be used in conjunction with the lattice parameter to yield a value for the wall thickness of the materials.

Characterization results

CeO_2: The high-angle powder X-ray diffraction pattern of the calcined samples shows well-resolved peaks characteris-

tic of crystalline CeO_2 (Figure 2a). The size of the CeO_2 crystalline domains calculated by using the Debye–Scherrer formula using the [111] peak reveals a particle size of ap-

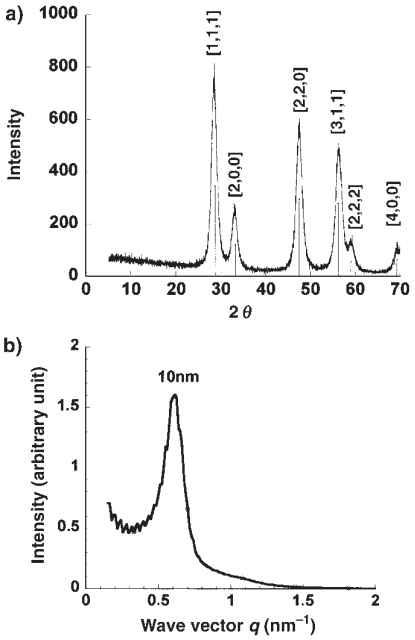

Figure 2. a) XRD pattern of the CeO_2 nanostructured material after calcination at 500 °C for 6 h. b) The SAXS pattern of the CeO_2 nanostructured material after calcination at 500 °C for 6 h.

proximately 4 nm. SAXS patterns of the as-synthesized nanostructured CeO_2 materials, after calcination at 500 °C for 6 h, show a peak centered at 10 nm (Figure 2b). Mesoscale order is confirmed by TEM images of the material calcined at 500 °C (Figure 3). Large, well-ordered channels, organized in hexagonal arrays, are clearly observed. The d_{SAXS} peaks can be indexed to a hexagonal cell with a unit-cell dimension a of 11.5 nm. Nitrogen adsorption–desorption isotherms were obtained for the calcined CeO_2 mesoporous sample (Figure 4). Analysis of the desorption curve suggests that the material possesses pores with a size of 5.5 nm. The

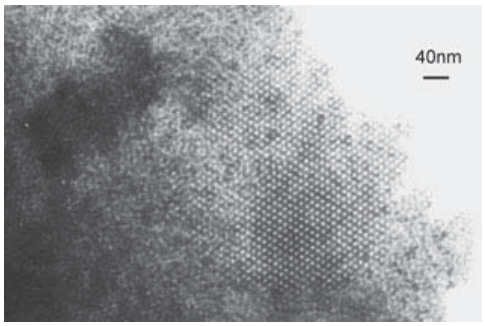

Figure 3. TEM image of the CeO_2 nanostructured material after calcination at 500 °C

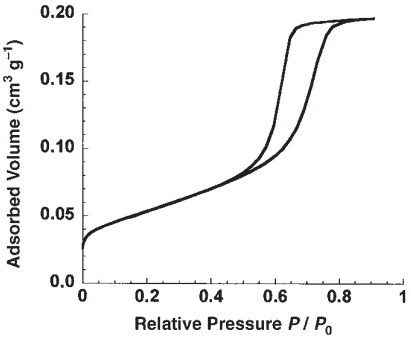

Figure 4. Nitrogen adsorption–desorption isotherms for the CeO_2 nanostructured material after calcination at 500 °C.

BET surface area and pore volume of the calcined materials are 125 $m^2 g^{-1}$ and 0.20 $cm^3 g^{-1}$, respectively. The SAXS and BET measurements are consistent with the TEM observations, suggesting a pore size of 5.5 nm and a wall thickness of approximately 6 nm.

ZrO_2: The SAXS pattern of nanostructured ZrO_2 after calcination at 500 °C (Figure 5) displays a peak centered at 7.6 nm and a shoulder at 4.4 nm, which is apparent in a log–log plot. They can be indexed to a hexagonal cell with $a =$ 8.8 nm. TEM images of the calcined material (Figure 6)

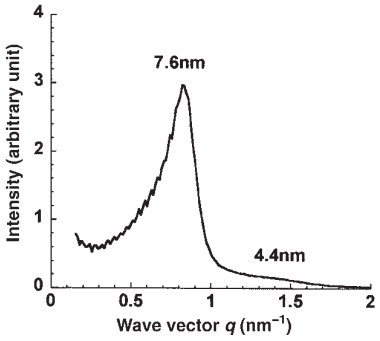

Figure 5. SAXS pattern of ZrO_2 nanostructured material after calcination at 500 °C for 6 h.

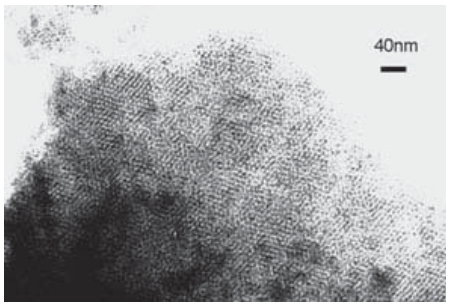

Figure 6. TEM image of the ZrO_2 nanostructured material after calcinations at 500 °C.

show hexagonal arrays of pores with the pores and walls possessing approximately the same size (4 nm). The high-angle XRD patterns recorded on these materials show well-resolved peaks characteristic of crystalline tetragonal ZrO_2, with minor peaks attributed to monoclinic ZrO_2. We determined a surface area of 180 $m^2 g^{-1}$ and an average pore size of 4 nm using nitrogen adsorption–desorption isotherms (Figure 7). Other characterization data are shown summarized in Table 1.

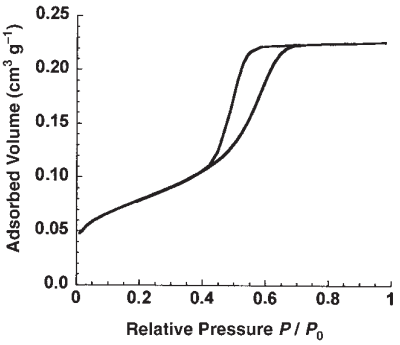

Figure 7. Nitrogen adsorption–desorption isotherms of the ZrO_2 nanostructured material after calcination at 500 °C.

Table 1. Summary of characterization data.

Material	Calcination temp. T [°C]	d_{SAXS} [nm]		Hex. unit cell length a [nm]	Pore size from BET [nm]	Wall thickness [nm]
CeO_2–5 nm	20	12.6	7.1	14.5		
	160	11.4	6.6	13.2		
	500	10	5.6	11.5	5.5	6
ZrO_2–3 nm	20	11.5	6.2	13.3		
	160	10.8	6.2	12.5		
	500	7.6	4.4	8.8	4	4.8
CeO_2–5 nm $Al(OH)_3$–3 nm[a]	20	13.2	7.3	15.2		
	160	12.6	7.2	14.54		
	500	11	6.5	12.7	9.5	3.2
CeO_2–5 nm $Al(OH)_3$–3 nm[b]	400	11		12.7	8	4.7

[a] Both surfaces modified. [b] Only the CeO_2 surface modified.

$Al(OH)_3$–CeO_2: Nanostructured composite materials formed from nanoparticles of $Al(OH)_3$ and CeO_2 were synthesized by using two procedures. The first involves the surface modification of the CeO_2 nanoparticles with aminocaproic acid and using $Al(OH)_3$ nanoparticles without surface modification. The aminocaproic surface-modified CeO_2 nanoparticles and $Al(OH)_3$ nanoparticles were mixed in a molar ratio $Al(OH)_3/(CeO_2 + Al(OH)_3)$ of 0.1:1. $Al(OH)_3$ nanoparticles are soluble in the acidic medium used to synthesize CeO_2 nanoparticle dispersions. After the amino acid post modification of the CeO_2 nanoparticles, the pH of the CeO_2 colloidal dispersion shifts to pH 4.5, allowing the stabilization of colloidal $Al(OH)_3$ nanoparticles and the resultant composites. These composites, formed with an [amino acid]/[CeO_2] ratio of 0.3:1, were calcined at 400 °C. From the SAXS pattern (Figure 8), we determined a d_{SAXS} value of 11 nm. TEM images of the composite show a hexagonal

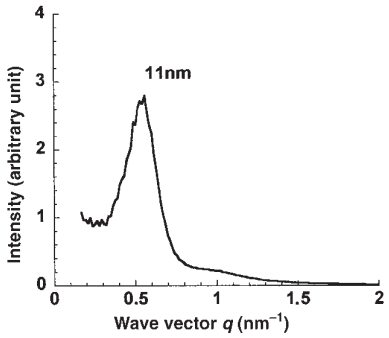

Figure 8. The SAXS pattern of $Al(OH)_3$ and aminocaproic acid modified CeO_2 composite material after calcination at 400 °C.

structure (Figure 9). The calcined materials showed a well-defined step in the N_2 adsorption–desorption isotherms (Figure 10), which indicates a material with a narrow pore size distribution. Surface area, pore diameter, and pore volume were 180 $m^2 g^{-1}$, 8 nm, and 0.32 $cm^3 g^{-1}$, respectively. The incorporation of Al and Ce into the nanostructured material is evidenced by EDS elemental analysis on thin sections of the calcined material, prepared by ultramicrotomy, and performed on 50-nm^3-sized domains. As $Al(OH)_3$ and CeO_2 are nonmiscible oxides, the observation of both Al and Ce in the small domains reveals the composite nature of the materials. The wall thickness is calculated as 4.7 nm, which is a size between that of the constituent

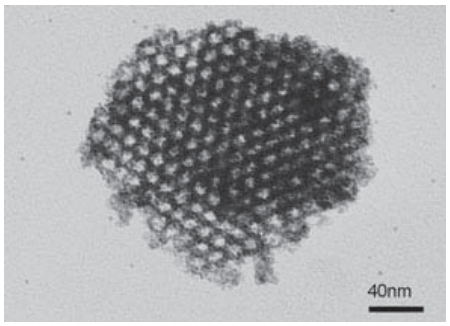

Figure 9. TEM image of the $Al(OH)_3$ and aminocaproic acid modified CeO_2 composite material after calcination at 400 °C.

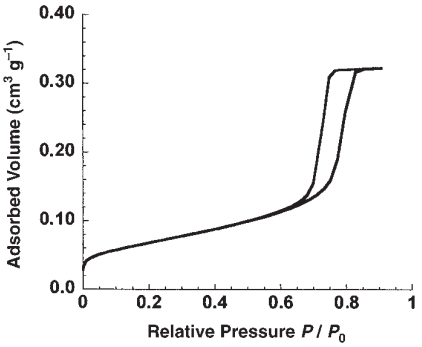

Figure 10. Nitrogen adsorption–desorption isotherms of the $Al(OH)_3$ and aminocaproic acid modified CeO_2 composite material after calcination at 400 °C.

CeO_2 and $Al(OH)_3$ nanoparticles, and suggests the presence of a monolayered material composed of the two types of nanoparticles.

$Al(OH)_3$-CeO_2: The second pathway to the formation of nanostructured composite materials involves amino surface modification of both CeO_2 nanoparticles (aminocaproic surface modification) and $Al(OH)_3$ nanoparticles (taurine surface modification). This preparation was performed to demonstrate the versatility of the surface modification mechanism, showing the synthesis of nanostructured composites materials from nanoparticle building blocks of different chemical compositions but displaying similar surface functionality. The aminocaproic surface-modified CeO_2 nanoparticles and taurine surface-modified $Al(OH)_3$ nanoparticles were mixed in a molar ratio $Al(OH)_3/(CeO_2 + Al(OH)_3)$ of 0.1:1. The materials formed after calcination at 500 °C have a hexagonal structure with peaks at 11 and 6.5 nm. The SAXS patterns are shown in Figure 11; the two peaks can be indexed to a hexagonal cell with lattice parameter of 12.7 nm. The high-angle XRD pattern displays well-resolved diffraction peaks attributed to the CeO_2 structure without the presence of peaks attributed to the aluminum compounds. The hexagonal structure was confirmed by TEM, which showed a hexagonal array of pores for the material calcined at 500 °C (Figure 12). BET adsorption curves (Figure 13) yield a pore diameter of 9.5 nm, a surface area

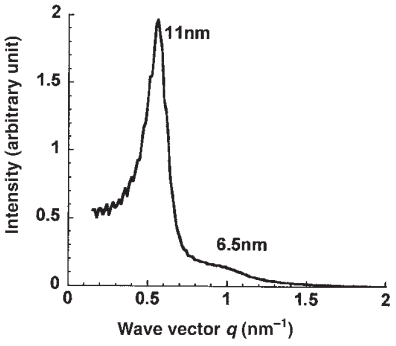

Figure 11. The SAXS pattern of the composite material made from aminocaproic acid surface-modified CeO_2 nanoparticles and taurine surface-modified $Al(OH)_3$ nanoparticles after calcination at 500 °C.

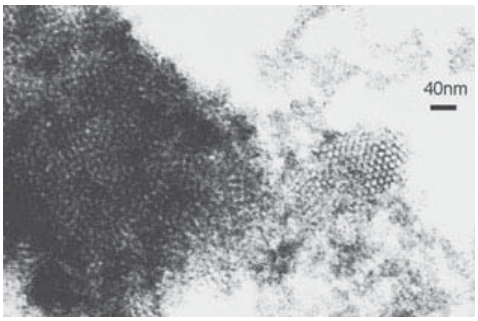

Figure 12. TEM image of the material made from aminocaproic acid surface-modified CeO_2 nanoparticles and taurine surface modified $Al(OH)_3$ nanoparticles showing an hexagonal array of pores after calcination at 500 °C.

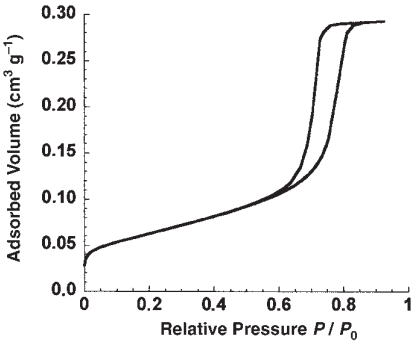

Figure 13. Nitrogen adsorption–desorption isotherms of the composite material made from aminocaproic acid surface-modified CeO_2 nanoparticles and taurine surface-modified $Al(OH)_3$ nanoparticles.

of 146 $m^2 g^{-1}$, and a pore volume of 0.29 $cm^3 g^{-1}$. The resultant calculated average wall thickness of 3.2 nm suggests that the nanostructure is formed from a monolayer of nanoparticles. These two routes allow the preparation of nanostructured composite materials composed of a regular juxtaposition of well-defined domains with sizes in the range of 3–5 nm.

The characterization data is summarized in Table 1.

Self-assembly of nanoparticles with liquid-crystal phases: We have investigated the detailed requirements and the mechanism for the self-assembly process on the liquid-crystal phase. Interactions between the nanoparticle surfaces and the block copolymer were probed for the CeO_2 nanoparticle system: the respective volumes of copolymer template and the nanoparticle were changed for a range of surface coverages of the nanoparticles by organic amines, by

adjusting the molar ratio [amine]/[CeO_2]. The experiments were conducted with the different poly(oxyalkylene) block copolymers, $EO_{20}PO_{70}EO_{20}$ and $EO_{100}PO_{70}EO_{100}$. Both copolymers possess the same block architecture with the same hydrophobic poly(propylene oxide) middle block but different hydrophilic poly(ethylene oxide) end-block sizes.

To monitor the relationship between the nanoparticle and copolymer volumes, we define the parameter Σ_v as the ratio of the copolymer volume ($V_{copolymer}$) to the total volume of the copolymer ($V_{copolymer}$) and the nanoparticles ($V_{nanoparticle}$), $\Sigma_v = (V_{copolymer})/(V_{copolymer} + V_{nanoparticle})$. This parameter, Σ_v, represents the copolymer volume fraction in the solid, dehydrated product. It can be determined by using the bulk densities of the copolymer and the nanoparticles. Σ_v is introduced as a useful tool in describing the three-phase system from which the nanoparticles assemble. Σ_v is related to the parameter Φ_v commonly used to describe volume fractions, defined as $\Phi_v = (V_{copolymer})/(V_{copolymer} + V_{nanoparticle} + V_{H_2O})$. V_{H_2O} is the volume fraction of H_2O and is not included in the definition of Σ_v. Since the nanostructured materials are formed by evaporation (a concentration step), the original H_2O concentration is not regarded as a critical parameter. An optimum value for Σ_v, designated *optimum* Σ_v, was defined for the sample with the most consistent nanostructure, that is, the sample with the highest proportion of nanostructured domains. The sample with the *optimum* Σ_v value is selected experimentally by an inspection of the first-order Bragg peak of the structure factor. The sample with the largest area under the first-order Bragg peak was assigned as being prepared at the *optimum* Σ_v value. The TEM images of the calcined samples were inspected to confirm a consistent nanostructure for the materials prepared at the *optimum* Σ_v value.

For the CeO_2 system, the carboxylic portion of the amino acid binds to the CeO_2 surface, exposing the amine group, which is subsequently protonated. Zhao et al[6] previously proposed a mechanism for the formation of structured silica surfaces in acidic media. The silica surfaces are described as $SiOH\cdots H^+$, interacting with copolymer EO moieties through a combination of electrostatic, hydrogen-bonding, and van der Waals interactions via the intermediate, $[(EO)H_3O^+]\cdots NO_3^-\cdots H^+-HOSi$. Our self-assembly process can involve the presence of long-range and strong repulsive electrostatic interactions between the nanoparticles, thus preventing homo-flocculation. After the addition of the copolymer, the nanoparticle dispersion remains colloidally stable, indicating the presence of weak interactions between the nanoparticle and the copolymer EO groups. Since our CeO_2 nanoparticle self-assembly process occurs in a mildly acidic pH range (pH 4–5) and without any added salts, we can propose a mechanism for the formation of nanostructured materials in which the protonated amino acid CeO_2 surfaces interact directly with the ethylene oxide (EO) groups of the copolymer, $CeO_2-NH_2\cdots H^+\cdots EO$. During the concentration step, capillary forces drive the nanoparticles together, resulting in an enhancement of short-range interactions between the copolymer EO group and the nanoparticle surfaces.

The [amino acid]/[CeO_2] molar ratio was adjusted to yield nanoparticles with varied amounts of surface coverage. The $[H^+]$/[EO] ratio was determined by assuming that all of the amino acid is protonated and bound to the CeO_2 surface. By using $EO_{20}PO_{70}EO_{20}$ and $EO_{100}PO_{70}EO_{100}$, the molar ratio of $[H^+]$/[EO] giving *optimum* Σ_v values was determined to be in the range 0.3 to 0.7, with [amino acid]/[CeO_2] molar ratios varying from 0.2 to 0.4.

Samples with *optimum* Σ_v, that is, with the largest proportion of nanostructures present, were observed by using an [amino acid]/[CeO_2] molar ratio of 0.3:1. Percentage surface coverages were calculated by assuming spherical CeO_2 nanoparticles with diameters of 5 nm, a CeO_2 bulk density of 7.13 $g\,cm^{-3}$, and carboxylic group binding areas of 25 $Å^2$. For the reaction conditions at which the [amino acid]/[CeO_2] molar ratio is 0.2:1, a surface coverage of the nanoparticle surface was calculated as 102%. However, CeO_2 nanoparticles possess a hydrated surface which diminishes the density of the nanoparticles compared to that of the bulk value. In addition, the nanoparticles have rough surfaces that increase their surface areas beyond the calculated values. These two factors bias the amino acid surface-coverage calculation, suggesting that full surface coverage occurs at a higher [amino acid]/[CeO_2] molar ratio closer to value of 0.3:1, which gives the greatest proportion of observed nanostructures. These calculations suggest that the conditions for self-assembly require a minimum surface coverage corresponding to one protonated -NH_2 group per 25 $Å^2$ of the nanoparticle surface. This low density of amino groups required for the self-assembly of nanoparticles can be compared to other nanoparticle self-assembly processes that operate through hydrogen bonds. The self-assembly of nanosized proteins along a RNA strand in nature involves double or triple hydrogen bonds between complementary bases with a higher density of interacting groups.[20]

Figure 14 shows the variation of the area under the first-order Bragg peak, used to determine the *optimum* Σ_v value, for the organic copolymers $EO_{100}PO_{70}EO_{100}$ and $EO_{20}PO_{70}EO_{20}$. The copolymer $EO_{100}PO_{70}EO_{100}$ with long hydrophilic EO chains forms materials with low *optimum* Σ_v

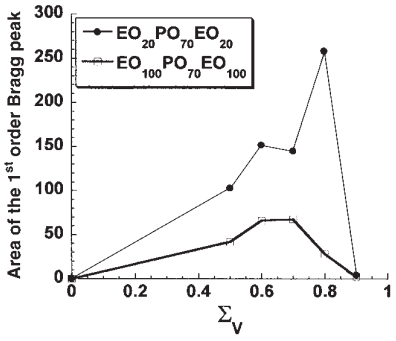

Figure 14. Variation of the area under the first-order Bragg peak, used to determine the *optimum* Σ_v for the organic copolymers $EO_{100}PO_{70}EO_{100}$ and $EO_{20}PO_{70}EO_{20}$.

values, whereas the corresponding large molar volumes of nanoparticles used gives rise to large wall thicknesses of 8 nm. Nanostructured materials are formed at higher *optimum* Σ_v values for $EO_{20}PO_{70}EO_{20}$, with a lower total volume fraction of nanoparticles. This gives rise to materials with wall thicknesses of 6 nm. This value is close to the 5 nm diameter of the nanoparticles, indicating that the nanostructure is constructed from a monolayer of nanoparticles. The results suggest that the preparation of nanostructured materials composed of a monolayer of nanoparticles requires a matching of the lengths of the hydrophilic EO moieties of the copolymer and the nanoparticle diameter. This matching has been achieved for the $EO_{20}PO_{70}EO_{20}$ copolymer, resulting in the monolayer thicknesses observed at the *optimum* Σ_v values discussed.

Different *optimum* Σ_v values were observed for the various nanoparticle systems used. These differences can be accounted for by considering the nanoparticle radii. By using a constant copolymer mass, identical numbers of EO potential anchoring sites are presented by the copolymer in the liquid-crystal phase. In a simplified scheme one may consider an equivalent copolymer surface instead of a number of anchoring sites. The ratio of the number of nanoparticles for the CeO_2 and ZrO_2 systems required to fully cover the copolymer surfaces is given by the relation $N_{CeO_2}/N_{ZrO_2} = r_{ZrO_2}^2/r_{CeO_2}^2$. This corresponds to a total volume of CeO_2 and ZrO_2 nanoparticles and can be defined by: $V_{CeO_2}/V_{ZrO_2} = r_{CeO_2}^3/r_{ZrO_2}^3 \times N_{CeO_2}/N_{ZrO_2} = r_{CeO_2}/r_{ZrO_2}$. Therefore, since r_{CeO_2} is greater than r_{ZrO_2}, we expect the *optimum* Σ_{ZrO_2} value to be greater than the *optimum* Σ_{CeO_2} value. This can be visualized by the smaller ZrO_2 nanoparticles arranged in a monolayer yielding a smaller wall thickness, having small nanoparticle volume fractions.

Rearrangement of the nanostructured arrays: Rearrangements of the nanostructured arrays occur during the calcination step. SAXS data of the dried samples were recorded at room temperature, 160 °C (before the total pyrolysis of the surfactant), and at 500 °C.

The SAXS characterization of the $EO_{20}PO_{70}EO_{20}$–CeO_2 material dried at 20 °C shows an intense peak centered at 12.6 nm and a less intense peak at 7.1 nm, compatible with a hexagonal cell with a lattice $a = 14.5$ nm. A log–log representation of the $I = f(q)$ curve of the SAXS data gives a significant shape factor at $q = 0.16$ Å^{-1}, confirming the presence of 5-nm-diameter, spherical CeO_2 nanoparticles in the dried material formed at 20 °C. A degree of contraction can be determined, $Q = (d_{saxs}^{T_1{}^\circ C} - d_{saxs}^{T_2{}^\circ C})/(d_{saxs}^{T_1{}^\circ C}) \times 100$, which demonstrates the effect of heating on the lattice parameter. After heating the CeO_2 nanostructured material to 160 °C, the SAXS pattern (Figure 15) shows peaks at 11.4 and 6.6 nm. This gives a degree of contraction of 10 %. Further heating of this material to 500 °C results in a total contraction of 21 %. The continuous broadening of the fundamental peak and the decrease in intensity of the less intense peak when calcining from 20 °C to 500 °C, as observed from the spectra recorded on samples calcined at 20, 160, and 500 °C, indicates a continuous rearrangement of the nanoparticles towards a less-ordered hexagonal structure.

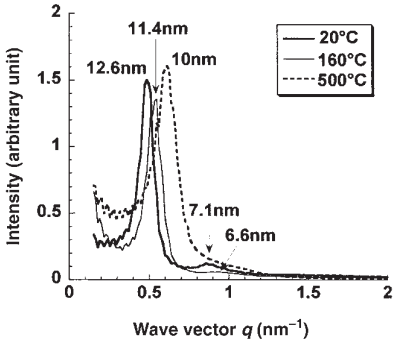

Figure 15. Comparison of the SAXS patterns of the dried and calcined CeO_2 materials

The SAXS patterns of the ZrO_2 and CeO_2–$Al(OH)_3$ materials, dried at 20 °C and calcined at 160 and 500 °C, exhibited peaks (data reported in Table 2) that were indexed to a similar hexagonal structure. All these nanostructured materials, whilst maintaining hexagonal symmetry, display a large degree of contraction upon heating from 20 to 500 °C. Contraction values of 21 % for the CeO_2 system, 35 % for the ZrO_2 system, and 17 % for the composite CeO_2–$Al(OH)_3$ material were observed. These suggest that the dried materials, formed at 20 °C, are not composed of nanoparticles that are closely packed on the surfaces of the copolymer.

The hexagonally nanostructured fully calcined materials formed from CeO_2 and ZrO_2 nanoparticles have a calculated wall thickness and pore size directly comparable to that of the diameter of the component nanoparticles; these values are summarized in Table 2. The SAXS and TEM data show that the uncalcined and calcined materials both exhibit a hexagonal structure. The SAXS data show that a reduction in unit cell volume occurs upon calcination. As a result of calcination the structure contracts to form a simple, more closely packed arrangement in which the nanoparticles are in close contact and occupy the vertices of a hexagon, resulting in pores of identical size (Figure 16). In this arrangement the six nanoparticles dictate a hexagonal symmetry in which

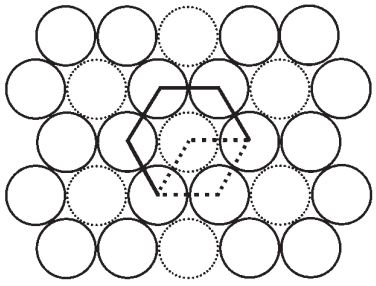

Figure 16. Simple arrangement of nanoparticles and pores in a hexagonal symmetry showing a pore size dictated by the diameter of the nanoparticles.

the wall thickness, pore size, and nanoparticle diameter are the same size. These observations suggest it may be possible to tailor materials to have specific pore sizes, wall thicknesses, and surface areas by carefully choosing the nanoparticle diameters.

The $(0.9)CeO_2$–$(0.1)Al(OH)_3$ material was prepared from a heterodisperse population of nanoparticles. For this heterodisperse population, an *optimum* Σ_v value was experimentally observed for a number of nanoparticles which corresponds to a high surface coverage of the copolymer when compared to the nanostructured CeO_2 material. During the concentration step the nanoparticle arrays undergo a smaller hexagonal cell shrinkage due to the large numbers of nanoparticles involved and their grouping together; this gives the dried material a large unit cell and pore size. These observations illustrate the effect of a heterodisperse population, both in terms of size and the number of nanoparticles, on the characteristics of the self-assembled arrays.

Conclusion

A versatile route has been developed for the formation of nanostructured materials from surface-modified nanoparticle building blocks by using a liquid-crystal template. Since our procedure involves interactions between a liquid-crystal template and an organic moiety through a surface modification of the nanoparticles, all nanoparticles, regardless of their composition, can be used to produce nanostructured materials with large surface areas. The versatility of this synthetic technique is exemplified by the formation of nanostructured materials from a mixture of nanoparticles of different chemical composition. The modification of the surfaces of $Al(OH)_3$ and CeO_2 nanoparticles with organic moieties leads to a mixture of nanoparticles that can be co-assembled with a liquid-crystal template to form a composite nanostructured material with a homogeneous distribution of $Al(OH)_3$ and CeO_2.

We propose a mechanism for the self-assembly of CeO_2 nanoparticles to form nanostructured materials. We have applied our method to synthesize a variety of nanostructured materials with hexagonal structures, in which the walls are composed of a monolayer of nanoparticles.

The rearrangement of the nanoparticles with temperature dictates the final characteristics of the nanostructured material. The symmetry of the arrays is preserved upon heating to temperatures greater than 500 °C. This rearrangement and contraction must be considered to design a specific nanostructured material. The size and heterodispersity of the nanoparticles initially involved in the arrays prepared at 20 °C was shown to influence some characteristics of the nanostructured arrays, such as pore diameter and surface area.

This route allows the formation of composite nanostructured materials that consist of a juxtaposition of discrete domains of nanoparticles composed of different oxides. These materials should possess new chemical and physical properties, which may occur as a consequence of the coupling effect of the different oxides at the nanometer scale, which in turn, should lead to a high density of hetero-interfaces and surface defects. These materials are therefore promising candidates as multifunctional materials in various fields, with potential applications as, for example, catalysts, optoelectronic materials, and absorbents.

Experimental Section

Chemicals and nanoparticle synthesis: Colloidal dispersions of 5-nm CeO_2 nanoparticles were prepared by the thermolysis of an acidified $Ce(NO_3)_4$ solution (0.5 M Ce^{4+}) followed by redispersion of the solid precipitate according to a method described in reference [21]. These dispersions, at pH 1, consisted of discrete CeO_2 nanoparticles that display a spherical morphology. Colloidal 3-nm amorphous ZrO_2 nanoparticles were purchased from the Nyacol Corporation. Colloidal dispersions of 3-nm $Al(OH)_3$ nanoparticles were synthesized by the controlled neutralization of an aqueous solution of aluminum chloride with urea, according to a method described in reference [22]. These dispersions (pH 4.8) contained nanoparticles with a spherical morphology. X-ray diffraction of the dried colloids showed a pattern similar to that for aluminum trihydroxide gels.[23]

The block-copolymer surfactants used include $HO(CH_2CH_2O)_{20}(CHCH_3CH_2O)_{70}(CH_2CH_2O)_{20}0H$ (designated $EO_{20}PO_{70}EO_{20}$, Pluronics P_{123} BASF), $HO(CH_2CH_2O)_{100}(CHCH_3CH_2O)_{70}(CH_2CH_2O)_{100}OH$ (designated $EO_{100}PO_{70}EO_{100}$, Pluronics F-127 BASF). These block copolymers are commercially available from Aldrich, BASF.

Synthesis of nanostructured materials: A typical synthesis of the nanostructured CeO_2 materials is outlined below. First, purification and concentration of the CeO_2 dispersion were performed by using an ultra-filtration cell equipped with a 3 kD cut-off membrane. Purification was monitored according to the residual acidity of the dispersion, determined by an acid titration of the supernatant after ultracentrifugation at 50 000 rpm for 6 h, and the concentration of ceria, measured by chemical analysis of the dried and calcined colloids. The desired molar ratio $[H^+]/[CeO_2]$ of 0.025:1 corresponds to a 4 M CeO_2 colloidal dispersion. Surface modification of the nanoparticles was then carried out by adding 6-aminocaproic acid $[H_2N(CH_2)_5CO_2H]$ (22.92 g) to the 4 M CeO_2 colloidal dispersion (125 mL) previously described, and making the volume up to 500 mL with deionized water. This dispersion was aged at 20 °C for 16 h, washed with two equivalent volumes of deionized water using an ultra-filtration cell, concentrated further, and adjusted to 1 M CeO_2. The molar ratio, [amino acid]/$[CeO_2]$, was 0.3:1 at pH 4.5. Poly(alkylene oxide) block copolymer P_{123} (0.56 g) was dissolved in a mixture containing H_2O (10 mL) and the 1 M CeO_2 aqueous colloidal dispersion (5.8 mL) pretreated with aminocaproic acid. The resulting homogeneous dispersion was allowed to evaporate in air in an open Petri dish at room temperature for two days. The resulting solid samples were yellow. The as-synthesized samples were calcined at 400–500 °C for 6 h using a programmable oven, heating in air at a rate of 1 °C min^{-1}.

A similar procedure was used for the preparation of the ZrO_2 and $Al(OH)_3$–CeO_2 nanostructured materials. The as-received ZrO_2 colloidal dispersion and the $Al(OH)_3$ dispersion previously described were washed with six equivalent volumes of deionized water by ultra-filtration. Taurine $(H_2N(CH_2)_2HSO_3)$ was added to the colloidal dispersions with a [taurine]/$[ZrO_2]$ or [taurine]/$[Al(OH)_3]$ molar ratio of 0.3:1. These solutions were aged at 20 °C for 16 h, washed with two equivalent volumes of deionized water and then further concentrated by ultra-filtration and adjusted to 1 M in terms of ZrO_2 or $Al(OH)_3$. The mixtures containing nanoparticles and copolymer were concentrated by evaporation, and the calcination steps were carried out as for the preparation of the CeO_2 samples. The respective masses of copolymer and volume of 1 M colloidal dispersions of metal oxides are given in Table 2.

Table 2. Optimum synthetic conditions required for the preparation of self-assembled nanostructured materials.

Nanoparticle	Diameter [nm]	Vol. of dispersion [cm^3]	Copolymer mass [g]	Surface modification	[Amino]/ [cation] mole	$Op\Sigma_v$[a]	Calcd temp. [°C]
CeO_2	5	5	0.48	CeO_2–aminocaproic acid	0.3	0.8	500
ZrO_2	3	5	0.94	ZrO_2–taurine	0.3	0.9	500
$Al(OH)_3$-CeO_2 $(Al:Ce)_{mole}=(0.1:0.9)$	3/5	0.5/4.5	0.48	$Al(OH)_3$ nonmodified CeO_2–aminocaproic acid	0.3	0.79	400
$Al(OH)_3$–CeO_2 $(Al:Ce)_{mole}=(0.1:0.9)$	3/5	0.5/4.5	0.48	$Al(OH)_3$–taurine CeO_2–aminocaproic acid	0.3	0.79	500

[a] The *optimum* Σ_v values were calculated by using the following theoretical densities values of 7.13, 5.89, and 2.42 for CeO_2, ZrO_2, and $Al(OH)_3$, respectively, and $d=1$ for $HO(CH_2CH_2O)_{20}(CHCH_3CH_2O)_{70}(CH_2CH_2O)_{20}OH$. The nanostructured materials were obtained at various *optimum* Σ_v values, depending on the nanoparticles used.

Characterization: All characterizations were performed on manually ground samples. SAXS data were collected by using a 2-m pinhole instrument fitted with a 2D gas-filled detector operating at a wavelength of 1.54 Å ($Cu_{K\alpha}$ radiation) at the Centre d'Etudes de Saclay, France. This instrument is fully described in reference [24]. In all cases isotropic scattering was observed. 2D SAXS images were radially averaged and a background subtraction was applied. In the case of pure CeO_2 materials, absolute scaling of the scattered intensity was performed by applying a methodology developed by Spalla et al.,[25] based on the calculation of the thickness of an equivalent nonporous layer of solid. For that purpose the attenuation coefficient involved in the Lambert–Beer equation of the pure CeO_2 was calculated at a wavelength of 1.54 Å. The proportion of nanostructured material was compared for samples on the basis of this absolute scaled intensity. The SAXS data were then deconvoluted by using a form factor derived from the initial CeO_2 nanoparticles to get the structure factor. Determination of the area of the first-order Bragg peak allowed a comparison of the nanostructured materials.

Transmission electron microscopy (TEM) images were obtained on a JEOL 1200 EX electron microscope operating at 120 keV. The samples for TEM were prepared by directly dispersing the powders onto carbon-coated copper grids. Energy-dispersive X-ray (EDS) spectra were acquired separately on an Inca Energy 300 system with a Philips CM30 TEM microscope (electron beam size 10–100 nm).

The nitrogen adsorption and desorption isotherms at 77 K were measured by using a Micromeritics ASAP 2000 system on samples dried overnight under vacuum at 200 °C. For the BJH (Barret–Joyner–Halenda model), the pore-size distribution was obtained from the analysis of the desorption branch of the isotherms.

High-angle X-ray powder diffraction spectra were obtained on a Philips PW 1800 diffractometer using $Cu_{K\alpha}$ radiation ($\lambda=1.54$ Å).

Acknowledgement

We are thankful to O. Spalla and O. Taché (Centre d'Etudes de Saclay) for their help with the SAXS experiments. We also thank E. Apra and J. M. Donetti for nitrogen adsorption studies, A. Vacher for SAXS and TEM preparations and experiments, and N. Ouillon for X-ray diffraction experiments.

[1] A. Corma, *Chem. Rev.* **1997**, *97*, 2373–2419.
[2] Y. J. Han, G. D. Stucky, A. Butler, *J. Am. Chem. Soc.* **1999**, *121*, 9897.
[3] Y. M. Xu, A. R. Ning, J. Zhao, *J. Coll. Interf. Sci.* **2001**, *235*, 66–99.
[4] A. Walcarius, C. Despas, P. Trens, M. J. Hudson, J. Bessiere, *J. Electroanal. Chem.* **1998**, *453*, 249.
[5] M. Mamak, N. Coombs, G. A. Ozin, *Adv. Funct. Mater.* **2001**, *1*, 59–63.
[6] D. Zhao, Q. Huo, J. Feng, B. Chmelka, G. D. Stucky, *J. Am. Chem. Soc.* **1998**, *120*, 6024–6036.
[7] P. Yang, D. Zhao, D. I. Margolese, B. F. Chmelka, G. D. Stucky, *Chem. Mater.* **1999**, *11*, 2813–2826.
[8] D. M. Antonelli, J. Y. Ying, *Angew. Chem.* **1995**, *107*, 2202–2206; *Angew. Chem. Int. Ed. Engl.* **1995**, *34*, 2014–2017.
[9] D. M. Antonelli, J. Y. Ying, *Angew. Chem.* **1996**, *108*, 461–464; *Angew. Chem. Int. Ed. Engl.* **1996**, *35*, 426–430.
[10] L. Y. Chen, S. Jaenicke, G. K. Chuah, *Microporous Mater.* **1997**, *12*, 323–330.
[11] U. Ciesla, S. Schacht, G. D. Stucky, K. Unger, F. Schuth, *Angew. Chem.* **1996**, *108*, 597–600; *Angew. Chem. Int. Ed. Engl.* **1996**, *35*, 541–543.
[12] S. Valange, J. L. Guth, F. Kolenda, S. Lacombe, Z. Gabelica, *Microporous Mesoporous Mater.* **2000**, *35–36*, 597–607.
[13] D. M. Lyons, K. M. Ryan, M. A. Morris, *J. Mater. Chem.* **2002**, *12*, 1207–1212.
[14] E. L. Crepaldi, G. J. de A. A. Soler-Illia, A. Bouchara, D. Grosso, D. Durand, C. Sanchez, *Angew. Chem.* **2003**, *115*, 361–365; *Angew. Chem. Int. Ed.* **2003**, *42*, 347–351.
[15] S. Mann, S. A. Davis, S. R. Hall, M. Li, K. H. Rhodes, W. Shenton, S. Vaucher, B. Zhan, *J. Chem. Soc. Dalton Trans.* **2000**, 3753–3763.
[16] S. A. Davis, M Breulmann, K. H. Rhodes, B. Zhang, S. Mann, *Chem. Mater.* **2001**, *13*, 3218–3226.
[17] S. A. Davis, N. H. Burkett, N. H. Mendelson, S. Mann, *Nature* **1997**, *385*, 420–423.
[18] M. Breulmann, S. A. Davis, S. Mann, H-P Hentze, M. Antonietti, *Adv. Mater.* **2000**, *12*, 502–507.
[19] M. S. Wong, E. S. Jeng, J. Y. Ying, *Nanolett.* **2001**, *1*, 637–642.
[20] T. M. Schuster, R. B. Scheele, M. L. Adams, S. J. Shire, J. J. Steckert, M. Potschka, *Biophys. J.* **1980**, *32*, 313–329.
[21] J. Y. Chane-Ching, *EP Patent* 208 580, **1987**.
[22] N. Idrissi-Kandri, A. Ayral, C. Guizard, H. El Ghadraoui El, L. Cot, *Mater. Lett.* **1999**, *40*, 52–58.
[23] D. Papee, R. Tertian, R. Biais, *Bull. Soc. Chim. Fr.* **1958**, 1301.
[24] T. Zemb, O. Taché, F. Né, O. Spalla, *Rev. Sci. Instrum.* **2003**, *74*, 2456–2462.
[25] O. Spalla, S. Lyonnard, F. Testard, *J. Appl. Crystallogr.* **2003**, *36*, 338–347.